

Article

Research on Modification of Fe₃O₄ Magnetic Nanoparticles with Two Silane Coupling Agents

Hongchao Cui^{1,2,3,*}, Jiajia Zhang^{1,2}, Jingjing Lu^{1,2}, Zhenkun Li^{1,2} and Decai Li^{1,2,4}¹ School of Mechanical, Electronic and Control Engineering, Beijing Jiaotong University, Beijing 100044, China² Key Laboratory of Vehicle Advanced Manufacturing, Measuring and Control Technology, Beijing Jiaotong University, Ministry of Education, Beijing 100044, China³ Beijing Key Laboratory of Flow and Heattransfer of Phase Changing in Micro and Small Scale, School of Mechanical, Electronic and Control Engineering, Beijing Jiaotong University, Beijing 100044, China⁴ State Key Laboratory of Tribology, Department of Mechanical Engineering, Tsinghua University, Beijing 100084, China

* Correspondence: hccui@bjtu.edu.cn

Abstract: As a novel functional nanomaterial, Fe₃O₄ magnetic nanoparticles (MNPs) modified by different surfactants have attracted and are attracting worldwide interest. In this research, we introduced two different silane coupling agents to modify Fe₃O₄ MNPs instead of a single surfactant to achieve complete coating and functionalization. The modification mechanism was also explained. Techniques such as TEM, XRD, FT-IR, TG-DSC, and VSM were applied to characterize the obtained modified Fe₃O₄ sample. From these techniques, the following information is obtained: The characteristic bands of TEOS and KH-792 were present in the FT-IR spectra and in the XPS plots of modified Fe₃O₄ MNPs, demonstrating that the silane coupling agents were present in the sample obtained after the modification. The TG analysis of the modified sample showed complete decomposition at 228 °C. The mass ratio of the sample obtained before and after the modification was close to 29:65. The XRD patterns show that the modified Fe₃O₄ MNPs possessed an identical reverse spinel crystal structure as an unmodified Fe₃O₄ sample. The modification decreased the saturation magnetization of Fe₃O₄ MNPs from 70.04 emu/g to 57.41 emu/g and the coating did not change the superparamagnetism of Fe₃O₄ MNPs.



Citation: Cui, H.; Zhang, J.; Lu, J.; Li, Z.; Li, D. Research on Modification of Fe₃O₄ Magnetic Nanoparticles with Two Silane Coupling Agents. *Magnetochemistry* **2023**, *9*, 1. <https://doi.org/10.3390/magnetochemistry9010001>

Academic Editor: Andrea Caneschi

Received: 18 November 2022

Revised: 5 December 2022

Accepted: 17 December 2022

Published: 21 December 2022



Copyright: © 2022 by the authors. Licensee MDPI, Basel, Switzerland. This article is an open access article distributed under the terms and conditions of the Creative Commons Attribution (CC BY) license (<https://creativecommons.org/licenses/by/4.0/>).

Keywords: Fe₃O₄; silane coupling agent; surface modification; TEOS; KH-792

1. Introduction

The Fe₃O₄ MNPs possess many special characteristics totally different from bulk substances, which have attracted interest both for its scientific values and technological applications. The functional materials have been exploited in many fields such as ferrofluids [1,2], magnetic record [3], biomedicine [4,5], catalyst [6], electronic technique [7], etc., owing to their unique strong superparamagnetism, high saturation magnetization, and good biological compatibility. Various applications require the introduction of special functional groups to realize new features. Moreover, Fe₃O₄ is prone to be oxidized to Fe₂O₃ and totally lose magnetism due to its high surface activity [8]. The functionalization of Fe₃O₄ MNPs by surfactants can meet the two requirements. Oleic acid [9], lauric acid [10], SDBS [11], PEG [12], etc., are common surfactants used to modify Fe₃O₄ MNPs. Additionally, all these surfactants are hydrocarbons and their chemical properties are active and easy to be dissolved by solvents, thus stripping from the Fe₃O₄ surface and losing the modification effect. Furthermore, Fe₃O₄ modified by these conventional surfactants lacks low temperature adaptability and biocompatibility, so its applications are limited. Recently, some scientists have applied silane coupling agent as a surfactant to modifying Fe₃O₄ MNPs.

In Chen's study, silane coupling agent KH550 was used to modify NdFe₁₂N_x magnetic powders and prevented the NdFe₁₂N_x powders from corrosion and oxidation to ensure

excellent durability and stability [13]. In Zhu's experiment, four types of silane coupling agents were used to modify HNTs/Fe₃O₄ composite respectively, and it was found that the anilino-methyl-triethoxysilane (KH-42)-modified HNTs/Fe₃O₄ composite exhibited the highest capacity for adsorption [14]. To enhance the dispersive capacity in organic solvents, KH-570 was used to modify nano-Sb₂O₃ particles by a covalent bond (Sb-O-Si) [15]. Fe₃O₄ was coated by silica via hydrolysis and the condensation of TEOS and the mean size was 216.9 nm. The mean size was 275 ± 16.1 nm and the saturation magnetization was 2.9 emu/g when using sodium citrate prior to coating with silica in stabilization. Subsequently, the surface of particles was functionalized by amine groups using N-(2-aminoethyl)-3-aminopropyltrimethoxysilane (KH-792). The results obtained by zeta potential revealed that the highest value of the isoelectric point change, indicating a more efficient surface functionalization, occurred when the KH-792 concentration of 90 mM was used [16]. In Abedi's study, a citric acid-modified isocyanate silane coupling agent (MMSN-NCO-CA) was used and the magnetic nanoparticles they synthesized with MMSN-NCO-CA were smaller in pore size by only 3.52 nm; this magnetic particle could be used in the medical field [17].

All these experiments mentioned above used a single silane coupling agent as a surfactant, since the application of mixed silane coupling agents has not been developed. When modified by a silane coupling agent, SiO₂ usually deposits on the surface of Fe₃O₄ MNPs and forms the core-shell structure, but it is difficult to continue functionalization on the SiO₂ surface. The chance of a further reaction to prepare other composites is restrained. At the same time, the excessive deposition of SiO₂ leads to a size increase in Fe₃O₄ MNPs, which is not conducive to the preparation of stable and suspended ferrofluid based on Fe₃O₄ MNPs. In this research, we introduced two silane coupling agents to modify Fe₃O₄ MNPs to solve these problems. The modification mechanism of silane coupling agents was explained and the properties of modified Fe₃O₄ were tested and analyzed.

2. Materials and Experiments

2.1. Materials

Ferrous sulfate (FeSO₄·7H₂O) and ferric trichloride (FeCl₃·6H₂O) were purchased from Xilong Scientific Co., Ltd. (Shantou, China). Absolute ethyl alcohol and ammonium hydroxide (25%) were procured from Beijing Chemical Industry Group Co., Ltd. (Beijing, China). The silane coupling agents TEOS (Tetraethyl orthosilicate) and KH-792 (N-(2-aminoethyl)-3-aminopropyltrimethoxysilane) were obtained from Beijing Chemical Industry Group Co., Ltd. (Beijing, China). and Yangzhou Wanhe Chemical Co., Ltd. (Yangzhou, China), respectively. The purity grades of the chemicals analytical reagent (AR) and used as received without further purification. The water used in all the experimental processes was deionized water (the resistivity is 18.2 MΩ.cm) filtered using an ultrapure water machine (PSDK2-20-C) in the lab.

2.2. Experiments

Co-precipitation [18,19] is a simpler, more tractable and efficient method to control the size and composition of Fe₃O₄ MNPs. Bare Fe₃O₄ MNPs synthesized using co-precipitation follow the chemical equation: $\text{Fe}^{2+} + 2\text{Fe}^{3+} + 8\text{OH}^- = \text{Fe}_3\text{O}_4 + 4\text{H}_2\text{O}$. Under certain reaction conditions, the chemical reaction continues, resulting in a size increase in bare Fe₃O₄ MNPs. Both TEOS and KH-792 are used as surfactants to coat the surface of bare Fe₃O₄ MNPs to terminate the co-precipitation chemical reaction of Fe₃O₄ MNPs and control the particle size. Considering Fe²⁺ will be partially oxidized into Fe³⁺ in the non-protective atmosphere, the mole ratio of Fe²⁺:Fe³⁺ was adjusted to 1:1.75. The color of iron salts dissolved with 25% ammonia added as a precipitant at less than 60 °C and by stirring immediately changed from reddish-brown to black. Under stirring for 20 min, bare Fe₃O₄ MNPs were generated at this stage. The Fe₃O₄ MNPs were washed with deionized water until pH = 9 and then dispersed in anhydrous ethanol, heating to 65 °C and adding TEOS and KH-792 into the

flask for 2 h with continuous stirring. The modified Fe₃O₄ MNPs were collected by magnet and obtained after washing, filtering, and drying.

2.3. Characterization

The morphology and composition of synthesized Fe₃O₄ nanoparticles were characterized by X-ray diffraction (XRD, Bruker D8, Berlin, Germany), Fourier transform infrared spectroscopy (FT-IR, Bruker VERTEX 70V, Woodlands, TX, America), and transmission electron microscopy (TEM, JEOL-2100, Japan Electronics Corporation, Tokyo, Japan), respectively. The size distribution was tested by Malvern Zatersizer Nano-ZS. The surface tension of silane coupling agents was tested using a JZ-200 surface tension meter. The contact angles were tested using a photographic process in the angle measurement method (HKCA-15 HARKE, Beijing, China, droplet 3 μ L). The Fe₃O₄ synthesized were diluted and ultrasonically dispersed for 20 min and tested using the Zatasizer Nano ZS90 laser particle size analysis from Malvern, UK. The magnetic property was tested using a vibrating sample magnetometer (VSM, Lakeshore 8604, Lexington, MI, America), the thermal behavior was tested using TG-DSC (Netzsch STA449F3, Selb, Germany), and the elementary composition was tested using X-ray photo-electron spectroscopy (XPS, PHI Quantera SXM, ULVAC-PHI, Chigasaki, Japan).

3. Results and Discussion

3.1. Research on Modification Mechanism of Two Silane Coupling Agents

The reaction model of silane coupling agent modification on the Fe₃O₄ surface can be divided into four steps, as shown in Figure 1.

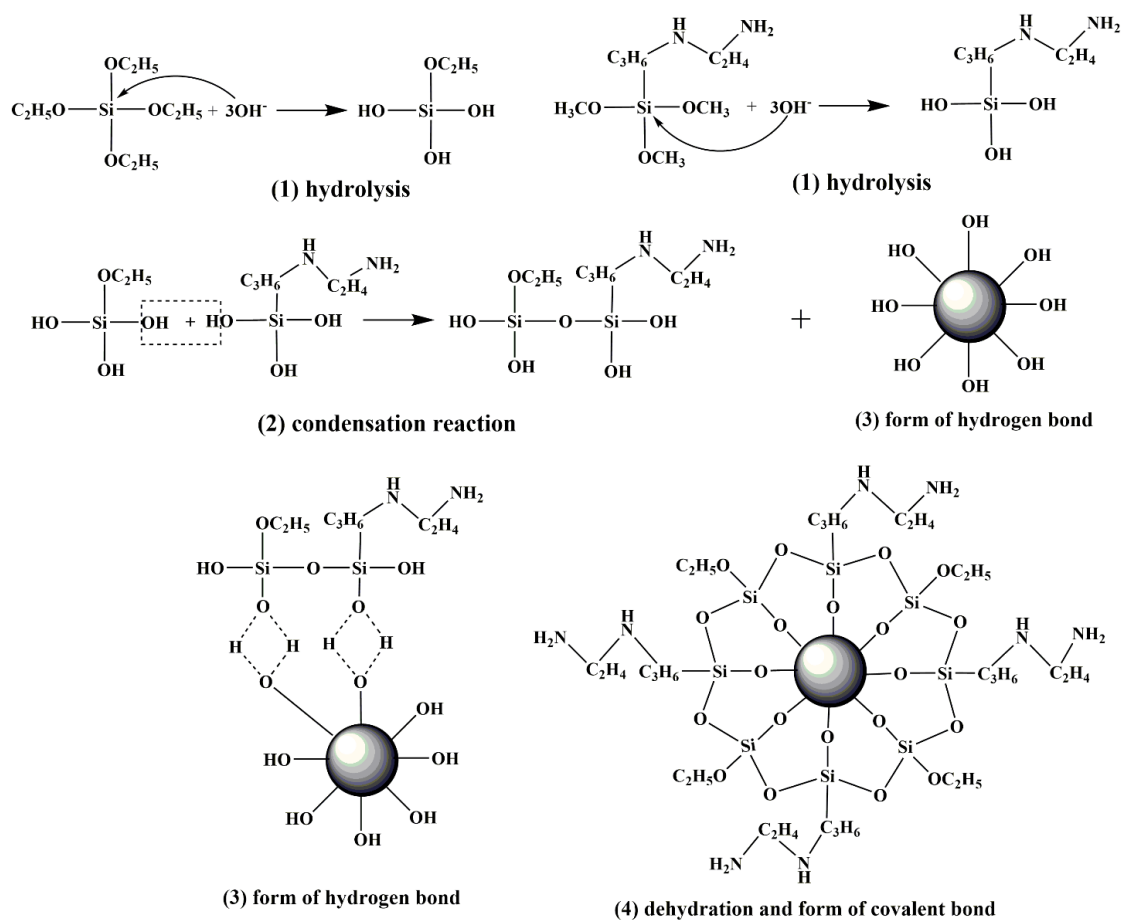


Figure 1. Modification mechanism of two silane coupling agent. (1) Hydrolysis; (2) Condensation reaction; (3) Form of hydrogen bond; (4) Dehydration and form of covalent bond.

(1) Hydrolysis: Silicon nucleus is negatively charged due to nucleophilic reaction of OH^- , leading to the shift of electron cloud to OC_2H_5 or OCH_3 , which weakens and breaks the Si-O bond. Si-OH is formed during the hydrolysis reaction. (2) Condensation reaction: $-\text{Si}(\text{OH})_3$ as a weak acid turns into an alkali after dehydrogenation in alkaline conditions. Dehydration polymerization occurs when nucleophilic attack is launched on silicon atoms. Polysiloxane (Si-O in main chain) with a low molecular weight is formed by dehydration condensation between the adjacent Si-OH of silanol. (3) Form of hydrogen bond: In aqueous solution, Fe_3O_4 shows Lewis acidity owing to the interaction between uncompleted 3d orbitals in Fe^{2+} and Fe^{3+} and lone-pair electrons in 2p orbitals in oxygen atom of H_2O [20]. The interaction reduces dissociation energy and weakens O-H bond in H_2O molecules, resulting in chemisorption of -OH on Fe_3O_4 surface [21]. Furthermore, hydrogen bond is formed between Si-OH in siloxane and -OH on Fe_3O_4 surface. (4) Dehydration and form of covalent bond: by continuous heating during the modification process, a covalent bond is formed between siloxane and -OH on Fe_3O_4 surface by dehydration reaction and finally stable coating is formed. It is generally believed that only one of the three -Si-OH is bonded with -OH on Fe_3O_4 surface and the other two have condensation reaction with -Si-OH in other silane or present a free state.

3.2. Thermal Stability Analysis

The experiment temperature of modified Fe_3O_4 was 25–350 °C and that of the unmodified Fe_3O_4 was 25–800 °C, as shown in Figures 2 and 3. The decomposition temperature of the silane coupling agents, oxidation of Fe_3O_4 , mass ratio, modification amount of silane coupling agent, and the thermal oxygen stability of Fe_3O_4 were obtained by studying the mass change, heat release, and absorption of Fe_3O_4 before and after modification.

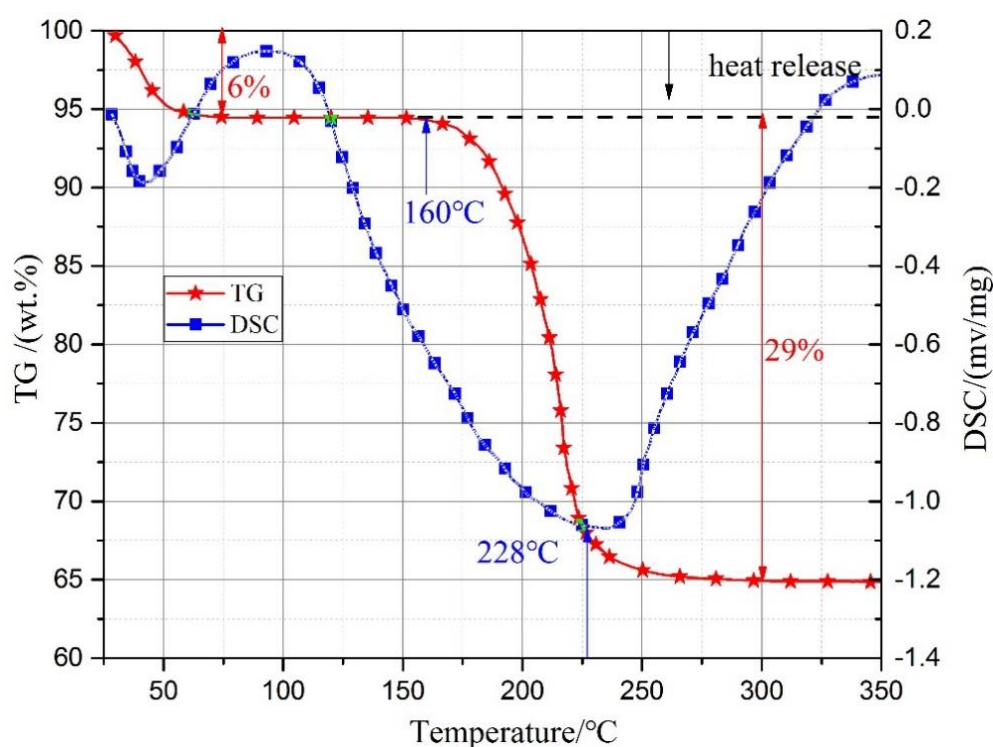


Figure 2. TG-SC curves of Fe_3O_4 modified by TEOS and KH-792.

From the two thermogravimetric loss curves, it can be seen that 6% and 7.2% weight losses were generated in the range of 25–100 °C, mainly from the water of hydration due to nanoscale surface active adsorption. Because of the hydrophobic effect of silane coupling agents, the adsorption water of modified Fe_3O_4 was slightly less than that of exposed Fe_3O_4 . The Fe_3O_4 modified by TEOS and KH-792 gradually produced about 29% weight

loss with the temperature increasing from 160 °C to 228 °C and simultaneously a large strong exothermic peak was formed in the DSC curve. The weight loss mainly resulted from heat a decomposition reaction of silane coupling agent under air atmosphere with volatile products generated such as NH_3 and CO_2 . The mass ratio of silane coupling agent to Fe_3O_4 core was 29:65. It is inferred that the applied temperature range of modified Fe_3O_4 was not higher than 228 °C.

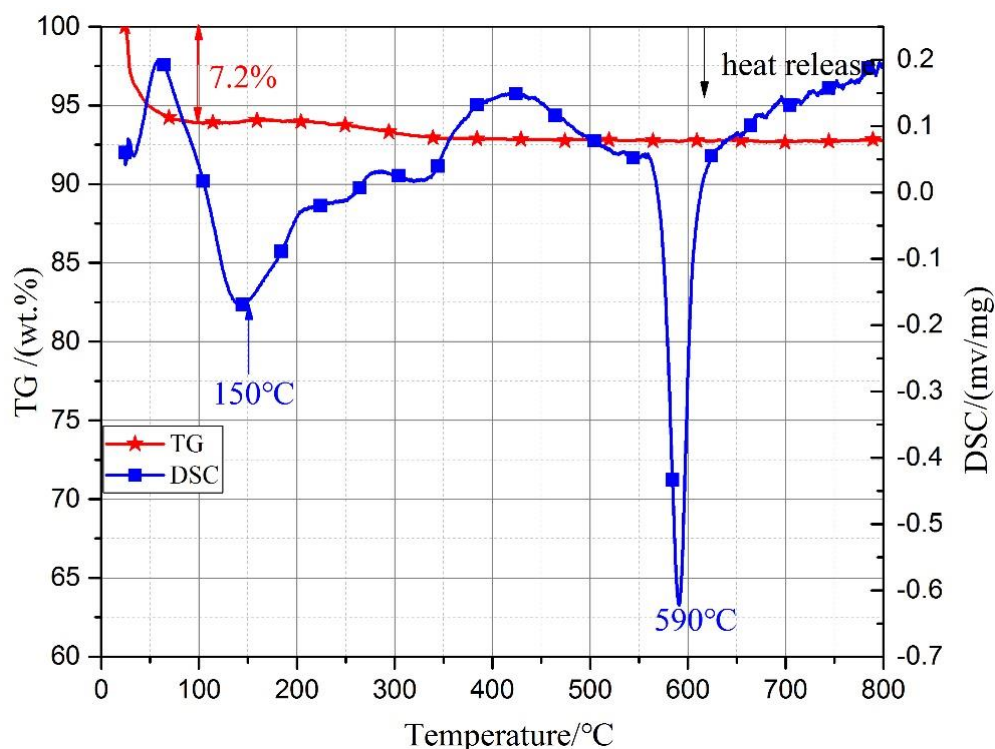


Figure 3. TG-DSC curves of Fe_3O_4 without modification.

However, there was no obvious mass loss at 150 °C and 590 °C in unmodified Fe_3O_4 as the temperature increased, but two strong exothermic peaks were caused by a phase transition of Fe_3O_4 [22]. Fe_3O_4 and $\gamma\text{-Fe}_2\text{O}_3$ are cubic systems and their lattice constants are very close. The oxidation of Fe_3O_4 to $\gamma\text{-Fe}_2\text{O}_3$ only increases the valence, that is, the Fe^{2+} changes to Fe^{3+} and there is no change in the position of the nucleus. However, $\alpha\text{-Fe}_2\text{O}_3$ is an orthorhombic system and its lattice constant is far from that of $\gamma\text{-Fe}_2\text{O}_3$ ($\alpha\text{-Fe}_2\text{O}_3$ lattice constant $a = 0.5034$ nm, while $\gamma\text{-Fe}_2\text{O}_3$ lattice constant $a = 0.8347$). When $\gamma\text{-Fe}_2\text{O}_3$ is transformed into $\alpha\text{-Fe}_2\text{O}_3$, the vacancies of Fe^{3+} and Fe^{2+} in the crystal cells both need to move greatly, the adjustment range is large, and more energy is released. In addition, the oxidation of Fe_3O_4 to $\gamma\text{-Fe}_2\text{O}_3$ and $\alpha\text{-Fe}_2\text{O}_3$ is a process of crystallization and the maximum exothermic peak appears at 590 °C. Our research showed that the superparamagnetism of Fe_3O_4 disappeared at 260 °C and only $\gamma\text{-Fe}_2\text{O}_3$ remained. When the temperature is higher than 650 °C, all the $\gamma\text{-Fe}_2\text{O}_3$ would turn into non-magnetic single $\alpha\text{-Fe}_2\text{O}_3$ [23]. According to the analysis of the TG–DSC curves, the silane coupling agent has been successfully modified on the Fe_3O_4 surface and its thermal-oxidative stability has been improved.

3.3. Component Analysis

(1) FT-IR spectroscopy analysis

The FT-IR spectroscopy of Fe_3O_4 MNPs modified by TEOS and KH-792 silane coupling agents is shown in Figure 4.

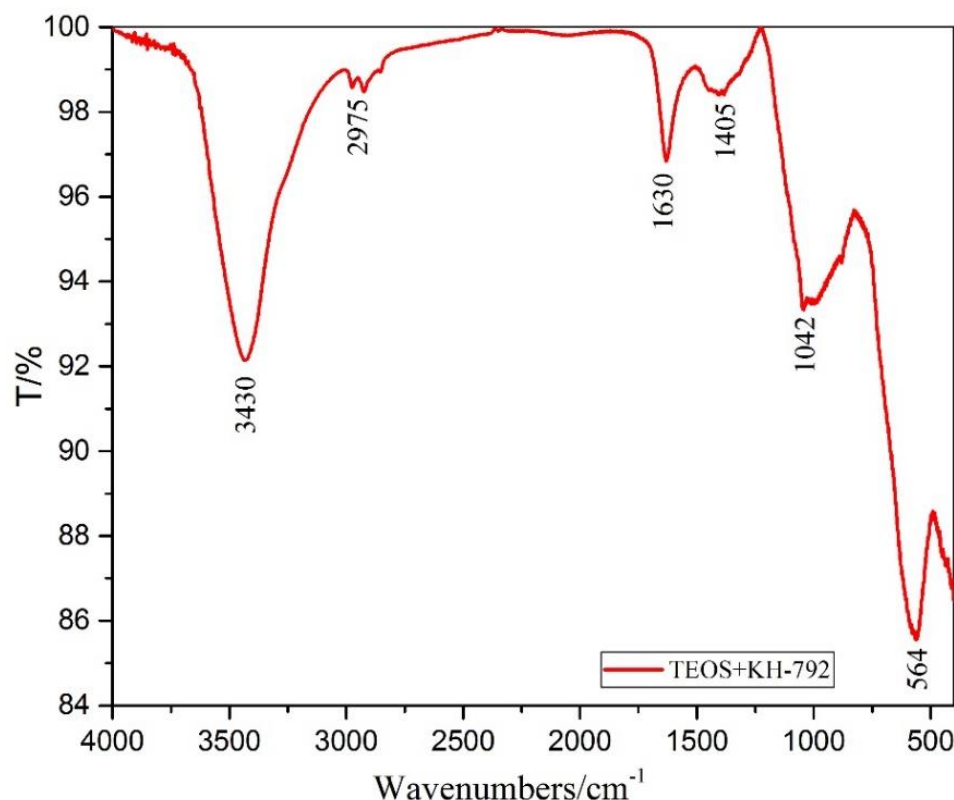


Figure 4. Infrared spectrum of Fe_3O_4 modified by TEOS and KH-792.

In the infrared spectrum, 564 cm^{-1} corresponds to the strong stretching vibration absorption peak of Fe-O in Fe_3O_4 [24]. Firstly, there is a large and strong absorption peak at 3430 cm^{-1} , which can be indexed to Si-OH. Si easily adsorbs -OH in an alkali solution after the breakage of Si-OC₂H₅ and Si-OCH₃. Secondly, the characteristic peak partly belongs to the -OH' stretching vibration absorption peak caused by the absorbed water on the Fe_3O_4 surface. Thirdly, the strong vibration absorption peak of N-H in KH-792 also strengthens the peak. The stretching vibration absorption peak of Si-O-Si is usually between $1029\text{--}1101\text{ cm}^{-1}$, for example 1042 cm^{-1} in this figure, which indicates that dehydration polymerization occurred between the two silane coupling agents; 1630 cm^{-1} is the in-plane bending vibration absorption peak of N-H in KH-792. The weak absorption peaks at 2975 cm^{-1} and 1405 cm^{-1} belong to the stretching vibration absorption peak and in-plane bending vibration absorption peak of C-H in -OCH₃ or -OCH₂CH₃ inside the chains of the silane coupling agent. The existence of C-H indicates that the -OCH₃ or -OCH₂CH₃ together with Si is only partially replaced by -OH. The characteristic peaks of Fe_3O_4 and silane functional groups appear simultaneously in the infrared spectrum of the sample, which indicates that the silane coupling agent has been successfully modified on the surface of Fe_3O_4 MNPs. The characteristic peaks of Fe_3O_4 and the silane coupling agent simultaneously exist in the infrared spectrum, which indicates that the two silane coupling agents have been successfully modified on the Fe_3O_4 surface.

(2) X-ray photoelectron spectroscopy analysis

The XPS photoelectron spectrum of Fe_3O_4 modified by TEOS and KH-792 silane coupling agents is shown in Figure 5.

The XPS analysis shows that the samples modified by TEOS and KH-792 mainly contained Fe, O, Si, C, N, and H. This is consistent with the elements in Fe_3O_4 MNPs and the silane coupling agent molecules. It proves that silane coupling agent has been successfully coated on the Fe_3O_4 surface. The main binding energies of the Fe2p spectrum are at 723.53 eV and 709.94 eV , which belong to the spectral band of Fe2p_{1/2} and Fe2p_{3/2} [12]. The

O1s spectrum with a binding energy of 529.20 eV is mainly composed of the lattice oxygen (O^{2-}) in the Fe_3O_4 and the -O- of the ether bond in the silane coupling agent. The energy spectra of $Si2p_{1/2}$ and $Si2p_{3/2}$ in Si2p appear at 101.21 eV and 92.98 eV; 284.31 eV represents C1s binding energy of $-CH_3$ or $-CH_2CH_3$ in the silane coupling agent; 391.88 eV is the binding energy of N1s in KH-792. The element contents obtained by XPS photoelectron spectroscopy are shown in Table 1.

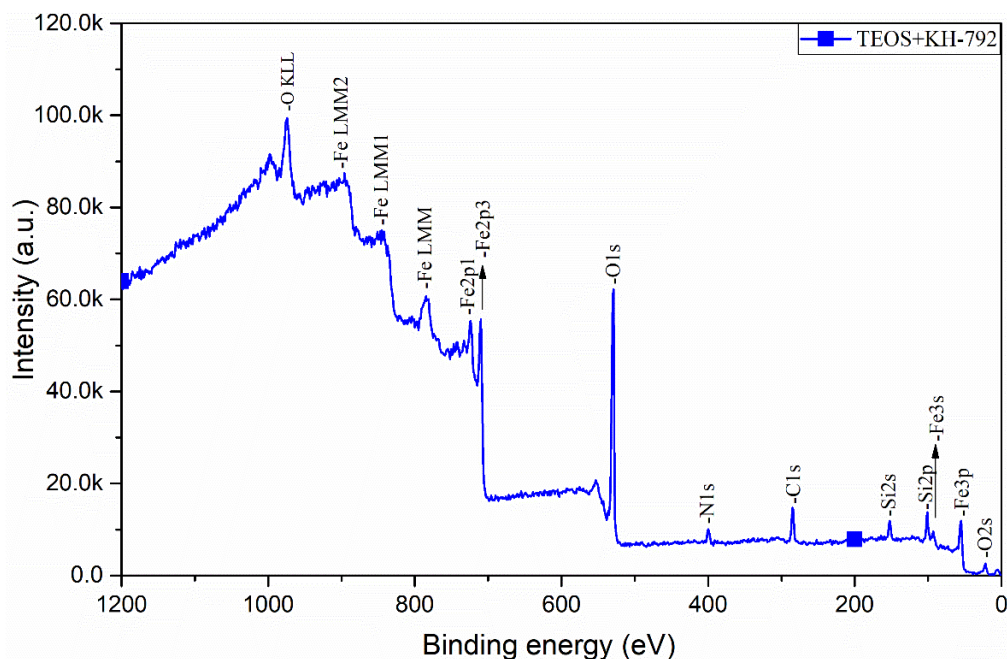


Figure 5. XPS photoelectron spectrum of Fe_3O_4 modified by TEOS and KH-792.

Table 1. Element contents of modified Fe_3O_4 after TEOS and KH-792.

Element	Fe2p	O1s	Si2p	C1s	N1s
Content	17.34	51.49	9.14	17.61	4.42

3.4. Crystal Structure

The XRD patterns of modified Fe_3O_4 MNPs are shown in Figure 6. The XRD pattern shows that there were obvious diffraction peaks at $2\theta = 30.0^\circ, 35.4^\circ, 43.1^\circ, 53.6^\circ, 56.9^\circ,$ and 62.4° corresponding to the crystal planes of Fe_3O_4 on (220), (311), (400), (422), (511), and (440), respectively. The position and intensity of the main diffraction peaks were basically consistent with the characteristic peaks of the PDF card (JCPDS 19-0629) [25]. The silane coupling agent was noncrystal and without diffraction peaks. The modification caused no change of the Fe_3O_4 crystal phase of the inverse spinel structure. The average grain size of the Fe_3O_4 nanoparticles modified by a silane coupling agent was approximately 9.7 nm as calculated by the Scherrer formula. $D_{hkl} = Nd_{hkl} = \frac{0.89\lambda}{\beta_{hkl} \cos \theta}$, λ is the X-ray wavelength of incident light; θ is the Bragg Angle of diffracted hkl; and β_{hkl} is the half-peak width of the diffracted hkl in radians. $K = 0.89$ and $Cu-K\alpha$, $\lambda = 0.15406$ nm. The silane coupling agent modified on the Fe_3O_4 surface formed an organic layer and prevented Fe^{3+} , Fe^{2+} , and OH^- from crystal growing, thereby controlling the particle size of Fe_3O_4 .

3.5. Micromorphology Analysis

The TEM patterns of Fe_3O_4 MNPs before and after modification with silane coupling agents are shown in Figure 7. It can be seen from the figure that the exposed Fe_3O_4 nanoparticles agglomerated seriously before modification and the boundary was not clear, as shown in Figure 7a. Most of the particles adhered to each other to form agglomerations,

which could not be dispersed by ultrasound. However, the Fe_3O_4 nanoparticles modified by the silane coupling agent were spherical and well-dispersed with a clear boundary, without adhesion and agglomeration, and the particle size decreased also. Before the addition of silane coupling agent, the precursor Fe^{3+} and Fe^{2+} were in an oversaturated state. The numerous crystal nuclei formed instantly when precipitant was added. The heat released by Fe_3O_4 crystal promoted the rapid growth of the crystal further. Moreover, the Fe_3O_4 particles agglomerated spontaneously to reduce the surface energy owing to the surface effect of the nanoparticles. Meanwhile, mutual attraction between magnetic dipole moments also led to continuous agglomeration. The addition of the silane coupling agent formed chemisorption on the Fe_3O_4 surface to terminate the co-precipitation reaction in time to prevent the continuous co-precipitation and the uncontrollable crystallization [26]. At the same time, the steric effect functioned on the Fe_3O_4 surface by the swing of the silane coupling agent hydrophobic chain, which inhibited the agglomeration of Fe_3O_4 and reduced Fe_3O_4 size, thereby achieving the purpose of controlling the particle size and distribution, as it shown in Figure 7b.

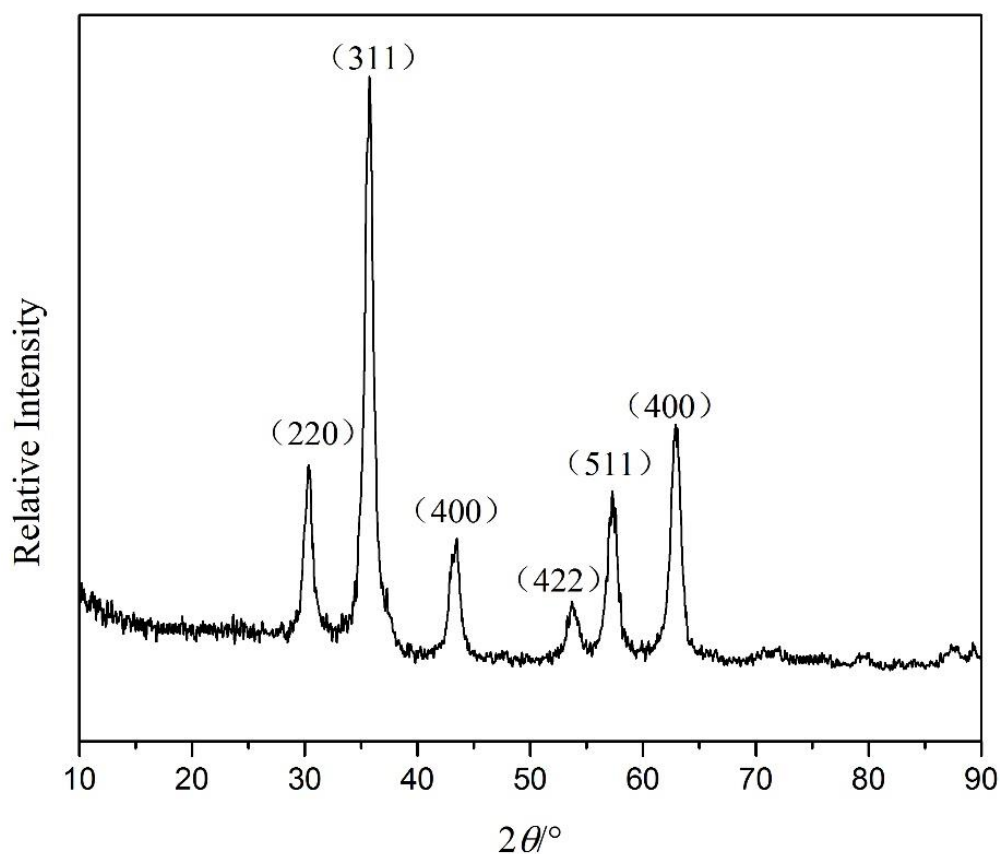


Figure 6. XRD patterns of Fe_3O_4 modified by TEOS and KH-792.

3.6. Particle Size and Size Distribution

Figure 8 shows the size distribution of Fe_3O_4 MNPs before and after modification of silane coupling agents. The size distribution of Fe_3O_4 without modification was mainly in the range of 20–40 nm and the average diameter was 30 nm. After modification, the size distribution was reduced to 7–15 nm significantly and the average diameter was 10 nm, consistent with the results calculated by XRD. The synthesis of Fe_3O_4 by co-precipitation was carried out in water. $\text{NH}_3 \cdot \text{H}_2\text{O}$ was used as a precipitant to process the crystallization reaction. Without a silane coupling agent, the Fe_3O_4 MNPs nucleated explosively and grew quickly, while when silane coupling agents were added, chemisorption occurred easily between nanoparticles and silane coupling agents. Then, the further chemical reaction of Fe_3O_4 was blocked by modification, thereby inhibiting the growth of particles.

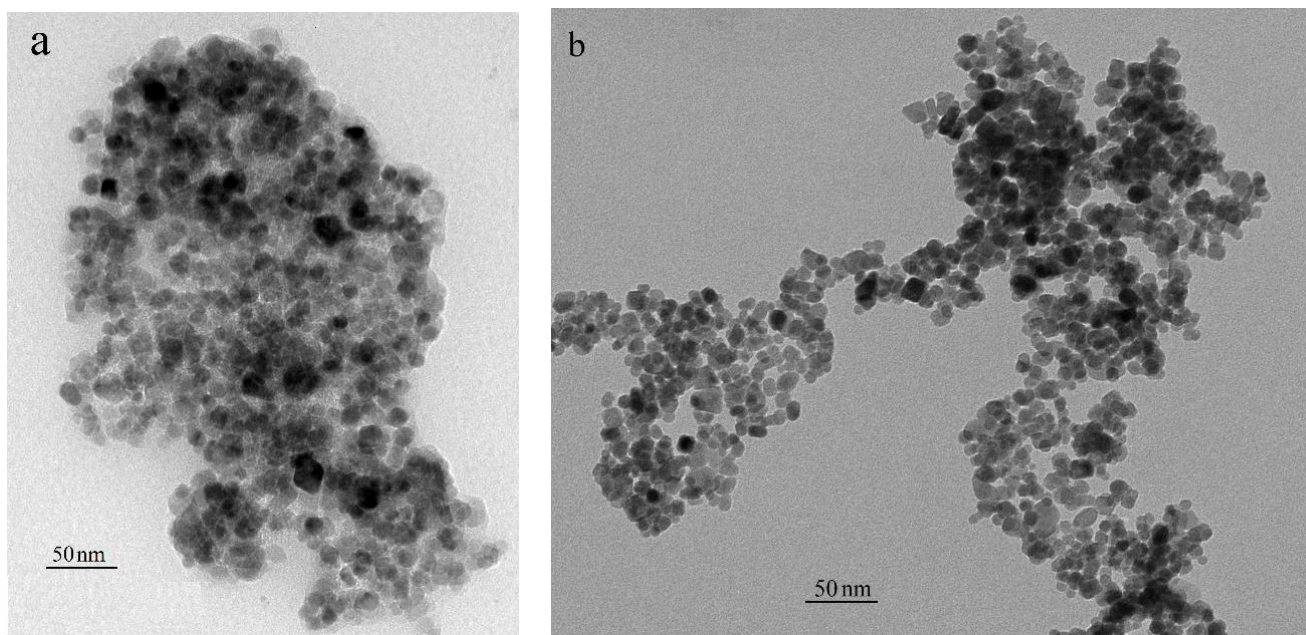


Figure 7. TEM patterns of Fe_3O_4 MNPs without (a) and with (b) modification by TEOS and KH-792.

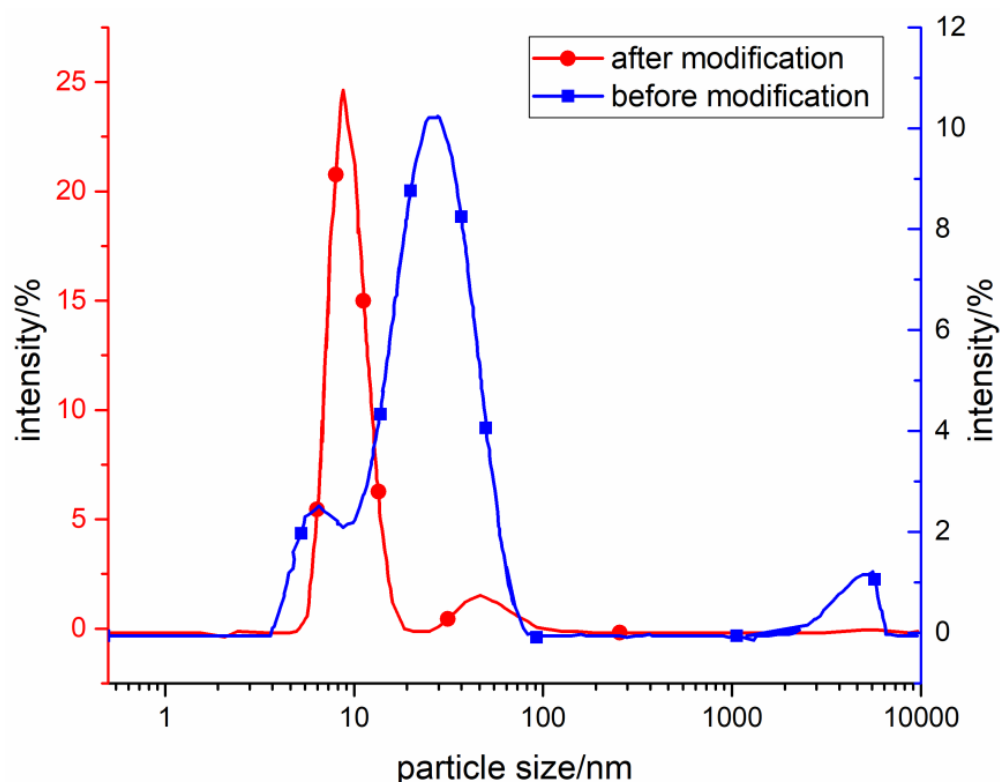


Figure 8. Size distribution of Fe_3O_4 MNPs before and after modification.

3.7. Low Surface Tension

The surface tension values of several surfactants are listed in Figure 9 [3]. Compared with hydrocarbon surfactants, the surface tension of KH-792 and TEOS was 24 mN/m and 25 mN/m, respectively, only slightly larger than the fluorocarbon surfactant. The siloxane side chain was perpendicular to the plane formed by the Si-O and could rotate or vibrate about the Si-O bond axis. Because the Si-O bond was longer, the hydrogen atoms on the alkyl group could be spread out similar to umbrellas. The rotation of the alkyl

groups occupied a large space and increased the distance between neighboring molecules. Meanwhile, due to the shielding effect of the alkyl group, the Si-O interaction was slight, molar volume was large, and surface tension was small [27]. This is the reason why the siloxane coupling agent was easy to spread on the Fe_3O_4 interface.

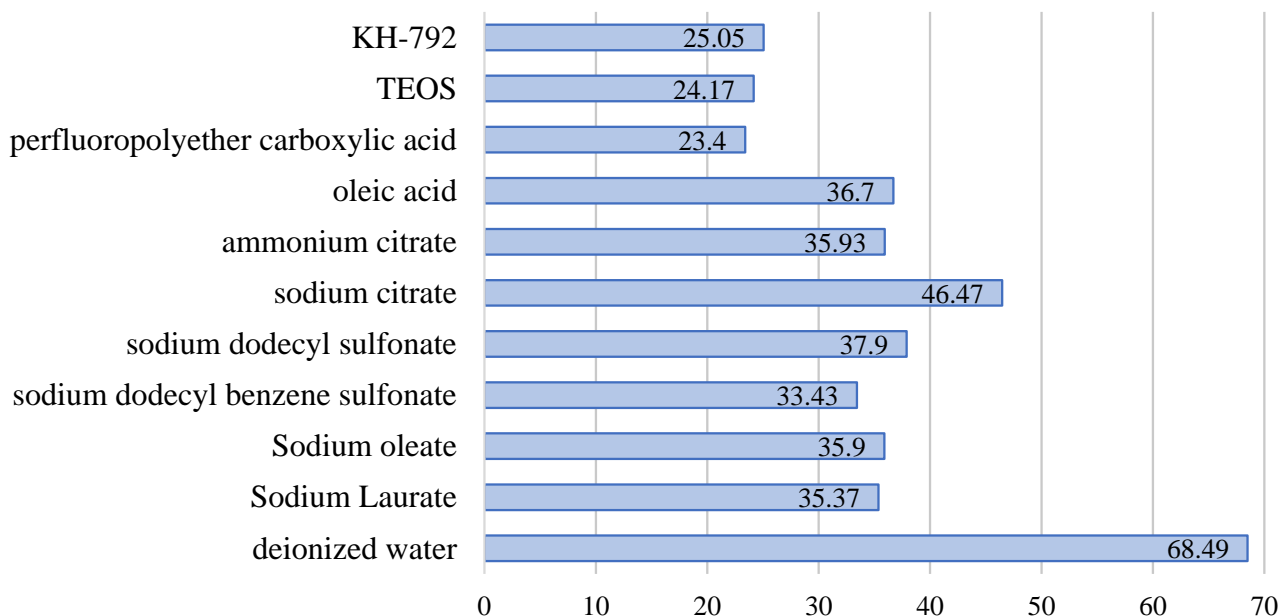


Figure 9. Surface tension values of several surfactants (mN/m).

3.8. Contact Angle

The photographic process was used in angle measurement, as shown in Figure 10, the contact angles of TEOS and KH-792 were 4.4° and 42.13° , respectively; they were less than 90° and could form a wetted surface with good hydrophilicity. This is the premise of the stable coating on Fe_3O_4 . The smaller the contact angle is, the faster it is to form wetting and spreading on the surface of nanoparticles and the easier it is to form a solid coating. Alkoxy in both KH-792 and TEOS's molecular chain can form a hydrogen bond with Fe_3O_4 nanoparticles, which can strengthen the force between the silane coupling agent and Fe_3O_4 nanoparticles.

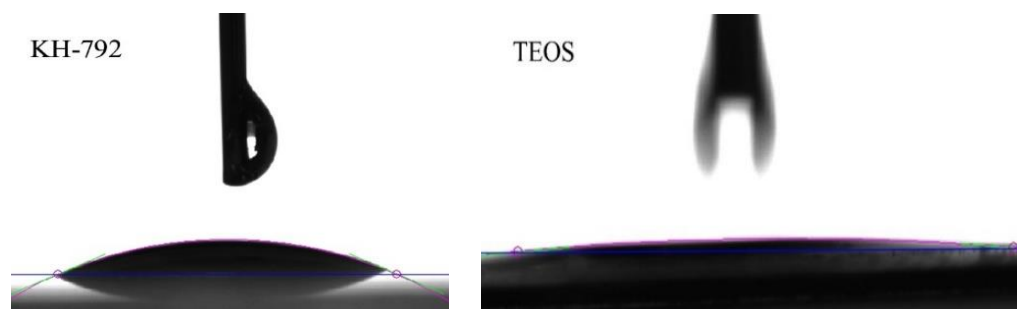


Figure 10. The photos of contact angles of TEOS and KH-792.

3.9. Magnetic Analysis

The hysteresis curves before and after modification with the silane coupling agent are shown in Figure 11.

It can be seen from the hysteresis curves that the coercivity and remanence of Fe_3O_4 approximate zero and the magnetization curves are similar to "S" either with or without modification, because the modification of the silane coupling agent does not change the superparamagnetism of Fe_3O_4 . The saturation magnetization of the bulk Fe_3O_4 was

92 emu/g [28], while that of the synthesized Fe_3O_4 MNPs without modification was 70.04 emu/g, which is mainly due to the fact that the nanometer size effect leads to the increase in the disordered atomic structure and decrease in the magnetic moment. The silane coupling agents slightly reduced the saturation magnetization to 57.41 emu/g after modification. There are three reasons for this: First, the silane coupling agents are non-magnetic material and the per unit mass of the magnetic material can be reduced [23]. Moreover, the interaction between Fe_3O_4 MNPs was weakened by modification. With the increase in nanoparticles in specific surface areas, the surface defects increased, meaning it was harder for magnetic moments to align in the direction of the magnetic field. This effect has been proved by other surfactants [29]. Finally, the magnetic performance is proportional to the particle size [30]. The growth of Fe_3O_4 was limited and particle size decreases due to the coating of the silane coupling agents, so the magnetization intensity was also decreased.

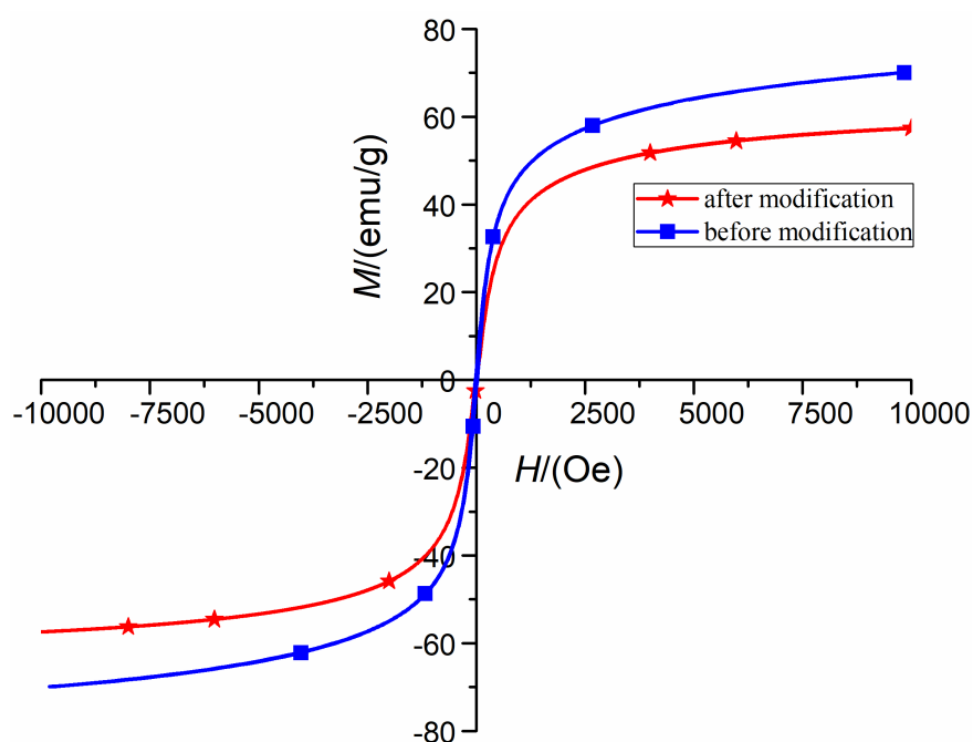


Figure 11. Hysteresis curves of Fe_3O_4 before and after modification.

4. Conclusions

The two silane coupling agents, TEOS and KH-792, were modified on Fe_3O_4 MNPs surface using hydrolysis, a condensation reaction, and dehydration. The silane coupling agents did not change the inverse spinel structure of Fe_3O_4 MNPs but could refine the grains. The average particle size decreased from 30 nm to 10 nm and the Fe_3O_4 MNPs were in homogeneous dispersion after modification. The characteristic peaks of TEOS and KH-792 were present in the FT-IR and XPS of the modified Fe_3O_4 MNPs, proving that silane coupling agents have been modified on the surface of Fe_3O_4 MNPs. The modification decreased the saturation magnetization of Fe_3O_4 MNPs from 70.04 emu/g to 57.41 emu/g and the superparamagnetism still remained. Additionally, the coating was completely decomposed at 228 °C. The mass ratio of coating to bare Fe_3O_4 was close to 29:65. Fe_3O_4 was partially transformed into $\gamma\text{-Fe}_2\text{O}_3$ near 150 °C and $\gamma\text{-Fe}_2\text{O}_3$ into $\alpha\text{-Fe}_2\text{O}_3$ near 600 °C. Over 680 °C, the Fe_3O_4 was finally oxidized to $\alpha\text{-Fe}_2\text{O}_3$ and lost its magnetic properties. The modified nanoparticles can be combined with polyethylene glycol, water-based cellulose, or other small molecules of silica gel to achieve potential applications in areas such as biomedicine, 3D printing, or soft robot development.

Author Contributions: Conceptualization, H.C.; Writing original draft, H.C.; Methodology, J.Z.; Review & editing, J.L. and Z.L.; Investigation, J.Z.; data curation, J.L.; Resources, H.C. and D.L.; Supervision, H.C. and Z.L. All authors have read and agreed to the published version of the manuscript.

Funding: This study has been supported by Beijing Natural Science Foundation (2222072), Foundation of Key Laboratory of Vehicle Advanced Manufacturing, Measuring and Control Technology (Beijing Jiaotong University), Ministry of Education, China (M21GY1300050), the Fundamental Research Funds for the Central Universities (2022JBMC032), and National Major Instrument Research and Development Program of Natural Science Foundation of China (51927810).

Institutional Review Board Statement: Not applicable.

Informed Consent Statement: Not applicable.

Data Availability Statement: All the data generated or analyzed during this study are included in this published article.

Conflicts of Interest: The authors declare no conflict of interest.

References

1. Yachi, T.; Matsubara, M.; Shen, C.; Asami, S.; Milbrandt, N.B.; Ju, M.; Wickramasinghe, S.; Samia, A.C.S.; Muramatsu, A.; Kanie, K. Water-Dispersible Fe₃O₄ Nanoparticles Modified with Controlled Numbers of Carboxyl Moieties for Magnetic Induction Heating. *ACS Appl. Nano Mater.* **2021**, *4*, 7395–7403. [\[CrossRef\]](#)
2. Mehrez, Z.; El Cafsi, A. Heat exchange enhancement of ferrofluid flow into rectangular channel in the presence of a magnetic field. *Appl. Math. Comput.* **2021**, *391*, 14. [\[CrossRef\]](#)
3. Frey, N.A.; Peng, S.; Cheng, K.; Sun, S. Magnetic Nanoparticles: Synthesis, Functionalization, and Applications in Bioimaging and Magnetic Energy Storage. *Chem. Soc. Rev.* **2009**, *38*, 2532–2542. [\[CrossRef\]](#) [\[PubMed\]](#)
4. Gao, L.Z.; Yan, X.Y. Nanozymes: Biomedical Applications of Enzymatic Fe₃O₄ Nanoparticles from In Vitro to In Vivo. In *Biological and Bio-Inspired Nanomaterials: Properties and Assembly Mechanisms*; Perrett, S., Buell, A.K., Knowles, T.P.J., Eds.; Springer: Berlin/Heidelberg, Germany, 2019; Volume 1174, pp. 291–312.
5. Lee, J.S.; Song, Y.J.; Hsu, H.S.; Lin, C.R.; Huang, J.Y.; Chen, J. Magnetic enhancement of carbon-encapsulated magnetite nanoparticles. *J. Alloy. Compd.* **2019**, *790*, 716–722. [\[CrossRef\]](#)
6. Guo, Z.W.; Adolfsson, E.; Tam, P.L. Nanostructured micro particles as a low-cost and sustainable catalyst in the recycling of PET fiber waste by the glycolysis method. *Waste Manag.* **2021**, *126*, 559–566. [\[CrossRef\]](#)
7. Guo, Y.; Zhang, D.Y.; Yang, Y.; Wang, Y.B.; Bai, Z.X.; Chu, P.K.; Luo, Y.S. MXene-encapsulated hollow Fe₃O₄ nanochains embedded in N-doped carbon nanofibers with dual electronic pathways as flexible anodes for high-performance Li-ion batteries. *Nanoscale* **2021**, *13*, 4624–4633. [\[CrossRef\]](#)
8. Han, J.; Wartenberg, M.G.; Chan, H.L.; Derby, B.K.; Li, N.; Scully, J.R. Electrochemical stability, physical, and electronic properties of thermally pre-formed oxide compared to artificially sputtered oxide on Fe thin films in aqueous chloride. *Corros. Sci.* **2021**, *186*, 109456. [\[CrossRef\]](#)
9. Zeng, Y.; Zhou, N.; Xiong, C.H.; Huang, Z.Y.; Du, G.P.; Fan, Z.Y.; Chen, N. Highly stretchable silicone rubber nanocomposites incorporated with oleic acid-modified Fe₃O₄ nanoparticles. *J. Appl. Polym. Sci.* **2022**, *139*, 51476. [\[CrossRef\]](#)
10. Nguyen, H.; Wang, Y.Z.; Moglia, D.; Fu, J.Y.; Zheng, W.Q.; Orazov, M.; Vlachos, D.G. Production of renewable oleo-furan surfactants by cross-ketonization of biomass-derived furoic acid and fatty acids. *Catal. Sci. Technol.* **2021**, *11*, 2762–2769. [\[CrossRef\]](#)
11. Choudhary, S.; Sachdeva, A.; Kumar, P. Time-based analysis of stability and thermal efficiency of flat plate solar collector using iron oxide nanofluid. *Appl. Therm. Eng.* **2021**, *183*, 13. [\[CrossRef\]](#)
12. Seal, P.; Alam, A.; Borgohain, C.; Paul, N.; Babu, P.D.; Borah, J.P. Optimization of self heating properties of Fe₃O₄ using PEG and amine functionalized MWCNT. *J. Alloy. Compd.* **2021**, *882*, 9. [\[CrossRef\]](#)
13. Chen, H.; Zheng, J.; Qiao, L.; Ying, Y.; Jiang, L.; Che, S. Surface modification of NdFe₁₂Nx magnetic powder using silane coupling agent KH550. *Adv. Powder Technol.* **2015**, *26*, 618–621. [\[CrossRef\]](#)
14. Zhu, K.; Duan, Y.; Wang, F.; Gao, P.; Jia, H.; Ma, C.; Wang, C. Silane-modified halloysite/Fe₃O₄ nanocomposites: Simultaneous removal of Cr(VI) and Sb(V) and positive effects of Cr(VI) on Sb(V) adsorption. *Chem. Eng. J.* **2017**, *311*, 236–246. [\[CrossRef\]](#)
15. Yang, W.; Shi, Z.; Li, M.; Zhang, Y.; Wang, Z. Surface Organic Modification of Nano-Sb₂O₃ Particles with Silane Coupling Agent. *Integr. Ferroelectr.* **2020**, *208*, 83–90. [\[CrossRef\]](#)
16. Mohammad-Beigi, H.; Yaghmaei, S.; Roostazad, R.; Bardania, H.; Arpanaei, A. Effect of pH, citrate treatment and silane-coupling agent concentration on the magnetic, structural and surface properties of functionalized silica-coated iron oxide nanocomposite particles. *Phys. E* **2011**, *44*, 618–627. [\[CrossRef\]](#)

17. Abedi, M.; Abolmaali, S.S.; Abedanzadeh, M.; Borandeh, S.; Samani, S.M.; Tamaddon, A.M. Citric acid functionalized silane coupling versus post-grafting strategy for dual pH and saline responsive delivery of cisplatin by Fe₃O₄/carboxyl functionalized mesoporous SiO₂ hybrid nanoparticles: A-synthesis, physicochemical and biological characterization. *Mater. Sci. Eng. C* **2019**, *104*, 109922. [[CrossRef](#)]
18. Slimani, S.; Meneghini, C.; Abdolrahimi, M.; Talone, A.; Murillo, J.P.M.; Barucca, G.; Yaacoub, N.; Imperatori, P.; Illes, E.; Smari, M.; et al. Spinel Iron Oxide by the Co-Precipitation Method: Effect of the Reaction Atmosphere. *Appl. Sci.* **2021**, *11*, 5433. [[CrossRef](#)]
19. Eskandari, M.J.; Hasanazadeh, I. Size-controlled synthesis of Fe₃O₄ magnetic nanoparticles via an alternating magnetic field and ultrasonic-assisted chemical co-precipitation. *Mater. Sci. Eng. B* **2021**, *266*, 115050. [[CrossRef](#)]
20. Joseph, Y.; Ranke, W.; Weiss, W. Water on FeO(111) and Fe₃O₄(111): Adsorption Behavior on Different Surface Terminations. *J. Phys. Chem. B* **2000**, *104*, 3224–3236. [[CrossRef](#)]
21. Breitbach, M.; Bathen, D.; Schmidt-Traub, H. Effect of Ultrasound on Adsorption and Desorption Processes. *Ind. Eng. Chem. Res.* **2003**, *42*, 5635–5646. [[CrossRef](#)]
22. Cornell, R.M.; Schwertmann, U. *The Iron Oxides: Structure, Properties, Reactions, Occurrences and Uses*; John Wiley & Sons: New York, NY, USA, 1996.
23. Cui, H.C.; Li, D.C.; Zhang, Z.L. Preparation and characterization of Fe₃O₄ magnetic nanoparticles modified by perfluoropolyether carboxylic acid surfactant. *Mater. Lett.* **2015**, *143*, 38–40. [[CrossRef](#)]
24. Lin, C.L.; Lee, C.F.; Chiu, W.Y. Preparation and Properties of Poly(acrylic Acid) Oligomer Stabilized Superparamagnetic Ferrofluid. *J. Colloid Interface Sci.* **2005**, *291*, 411–420. [[CrossRef](#)] [[PubMed](#)]
25. Xu, Z.c.; Hou, Y.l.; Sun, S.h. Magnetic Core/Shell Fe₃O₄/Au and Fe₃O₄/Au/Ag Nanoparticles with Tunable Plasmonic Properties. *JACS* **2007**, *129*, 8698–8699. [[CrossRef](#)]
26. Maity, D.; Agrawal, D.C. Synthesis of Iron Oxide Nanoparticles Under Oxidizing Environment and Their Stabilization in Aqueous and Non-aqueous Media. *J. Magn. Magn. Mater.* **2007**, *308*, 46–55. [[CrossRef](#)]
27. Bhattacharya, S.; Gao, Y.; Korampally, V.; Othman, M.T.; Grant, S.A.; Gangopadhyay, K.; Gangopadhyay, S. Mechanics of plasma exposed spin-on-glass (SOG) and polydimethyl siloxane (PDMS) surfaces and their impact on bond strength. *Appl. Surf. Sci.* **2007**, *253*, 4220–4225. [[CrossRef](#)]
28. Liao, M.H.; Chen, D.H. Preparation and Characterization of a Novel Magnetic Nano-adsorbent. *J. Mater. Chem.* **2002**, *12*, 3654–3659. [[CrossRef](#)]
29. Yamaura, M.; Camilo, R.L.; Sampaio, L.C.; Macedo, M.A.; Nakamura, M.; Toma, H.E. Preparation and Characterization of (3-aminopropyl) Triethoxysilane-coated Magnetite Nanoparticles. *J. Magn. Magn. Mater.* **2004**, *279*, 210–217. [[CrossRef](#)]
30. Peddis, D.; Cannas, C.; Musinu, A.; Piccaluga, G. Magnetism in Nanoparticles: Beyond the Effect of Particle Size. *Chem.-A Eur. J.* **2009**, *15*, 7822–7829. [[CrossRef](#)]

Disclaimer/Publisher's Note: The statements, opinions and data contained in all publications are solely those of the individual author(s) and contributor(s) and not of MDPI and/or the editor(s). MDPI and/or the editor(s) disclaim responsibility for any injury to people or property resulting from any ideas, methods, instructions or products referred to in the content.